Local-field effects in pattern formation in large-aspect-ratio lasers

Oscar G. Calderón, Eduardo Cabrera, M. Antón, and J. M. Guerra
Departamento de Optica, Universidad Complutense, Ciudad Universitaria s/n, 28040 Madrid, Spain
(Received 5 June 2002; revised manuscript received 19 November 2002; published 22 April 2003)

Transverse effects in the laser dynamics due to near dipole-dipole interactions are studied considering the presence of permanent electric dipole moments. The semiclassical two-level Maxwell-Bloch equations are used and a single longitudinal mode is assumed. A traveling wave is selected at threshold when the sum of the cavity detuning and the near dipole-dipole parameter is larger than zero. As a consequence of this, transverse pattern can occur even when the laser frequency is larger than the frequency of the atomic transition. Also, a cutoff in the laser field spectrum arises. We found that the near dipole-dipole interactions significantly modify the stability picture of the traveling waves. Numerical simulations have been carried out and the effect of the near dipole-dipole on the pattern formation is addressed.

DOI: 10.1103/PhysRevA.67.043812 PACS number(s): 42.60.Mi, 42.60.Jf, 42.50.Fx, 42.70.Hj

I. INTRODUCTION

Pattern formation and related transverse effects in lasers and other systems have been a field of intense research in recent years [1–11] (see also special issue in Ref. [12]). The single-longitudinal-mode laser has been a useful laboratory for the study of transverse phenomena without the influence of other degrees of freedom [2]. The control parameter that determines the mechanism which gives rise to structure formation is the Fresnel number (the aspect ratio of a nonlinear optical system) [4]. If the Fresnel number is low (under $\simeq 10$), the optical resonator imposes the geometry of the laser field which can be expanded on a suitable basis of empty cavity modes. However, as Fresnel number increases, the behavior of the system becomes more and more boundary-free, and the structure formation begins to be dominated by bulk parameters and nonlinearities of the active medium. In large-aspect-ratio (or large Fresnel number) homogeneously broadened two-level lasers, it is well known that the pattern selected just above threshold depends on the sign of the cavity detuning δ [1,7,13,14]. For negative detuning (cavities tuned above resonance), the laser selects a transverse spatially homogeneous solution, whereas for positive detuning (cavities tuned below resonance), a traveling wave is selected. In this last case, the laser emission is off-axis which helps the laser to emit on resonance. This phenomenon has been experimentally observed [15,16].

All these works have been done on the framework of the two-level Maxwell-Bloch equations, and the interactions between atoms, which are manifested through dipole-dipole interactions, have been ignored. This is generally accurate for large interatomic separations and low dipole moments. However, when the atomic system is working near resonance, the atoms can acquire a large dipole moment. Moreover, there are many molecular systems possessing large permanent dipole moments. A description of some materials with large permanent dipole moments can be found in Ref. [17]. The inclusion of the local-field correction (LFC) in the Maxwell-Bloch equations leads to a nonlinear relationship between the macroscopic susceptibility and the microscopic polarizability, and leads to many interesting phenomena such as self-phase modulation in self-induced transparency [18,19], linear and nonlinear spectral shifts [20,21], and novel inversion and ultrafast switching effects [22]. Maki *et al.* [21] measured the optical response of a dense potassium vapor and demonstrated that the densities required for the local-field effect to be important are not large. Thus, for example, a density of the sodium atoms around 10^{17} cm^{-3} gives a shift of about 1 GHz of the sodium *D* line [21]. Another interesting phenomenon induced by the LFC is the so-called intrinsic optical bistability (IOB) that was investigated in several works [23–26]. Hehlen *et al.* experimentally showed the IOB using Yb^{3+} ions in a $Cs_3Y_2Br_9$ crystal [27,28]. As a result of the introduction of LFC, the Bloch equations become nonlinear with respect to the population inversion and polarization amplitude. This nonlinear term can be interpreted as a detuning depending on the population inversion and leads to the appearance of IOB, i.e., the bistable dependence of the atomic variables on the intensity of the applied field.

The LFC has been also taken into account on the temporal dynamics of lasers. Sanchez *et al.* [29] and Fromager *et al.* [30] have recently studied the effects of local-field correction on the laser instabilities in homogeneously broadened media. They found that the LFC significantly reduces the instability threshold. A similar result was reported by Bowden *et al.* in the case of inhomogeneously broadened lasers [31]. Recently, Ahufinger *et al.* have included the laser field diffraction to analyze the spatiotemporal dynamics of broad-area lasers with the presence of LFC [32,33]. They showed that the transverse spatial dependence destroys the intrinsic bistability. They also found cavity solitons by using a Fourier filter.

Clearly, all of the above works suggest that it is important to understand the influence of the local-field effect on the laser transverse dynamics since it is very sensitive to detuning. For this reason, in the present work we assess theoretically the modifications on the pattern formation in large-aspect-ratio homogeneously broadened two-level lasers originated by the local-field correction. The description is made by means of semiclassical two-level Maxwell-Bloch equations, assuming a single longitudinal mode and the rotating wave and the slowly varying amplitude approximations. We also study the case where the active molecules present electrical permanent dipole moments [34]. The neutral stability curve obtained in the linear stability analysis of

the nonlasing state presents some features that are similar to those obtained in the case of a Raman laser model [7]. In our case, the curve depends on the near dipole-dipole (NDD) dimensionless parameter b that can take positive or negative values depending on the relevance of the permanent dipole moments. A traveling wave is selected when the sum of the cavity detuning and the NDD parameter is larger than zero ($\delta+b>0$) and its wave vector depends on the NDD strength. We find a lower cutoff when $b>0$ (an upper cutoff when $b<0$) in the laser field spectrum that gives the maximum (minimum) spatial scale that can appear in the transverse pattern. We have calculated the Busse balloon, that is, the region of stability of traveling waves and compared it to the standard one [7,14]. We found at positive NDD parameter that the near dipole-dipole interactions removes the Busse balloon, i.e., there is not any stable travelling wave. On the other hand, at negative NDD parameter, the nature of the instability boundaries changes since the Busse balloon is delimited by amplitude instabilities. We have also performed numerical simulations to observe the pattern formation above threshold. The simulations reveals that a more complex pattern formation takes place when the LFC is considered.

The paper is organized as follows: In Sec. II we present the two-level Maxwell-Bloch equations when the local-field correction is taken into account. We have also considered the presence of active molecules with permanent dipole moments. In Sec. III, we analyze how the new term affects the first laser threshold by making a detailed analysis of the nonlasing solution. The lasing solutions above threshold and their stability analysis are presented in Sec. IV. The numerical simulations are presented in Sec. V. Finally, Sec. VI provides brief conclusions.

II. LASER EQUATIONS

The starting point for our analysis are the Maxwell-Bloch equations for a large-aspect-ratio homogeneously broadened two-level laser with plane and parallel mirrors in the rotating wave, slowly varying amplitude, and single-longitudinal-mode approximations, and taking into account the LFC [29,30,35,36]. This system of equations was previously derived by Sánchez *et al.* [29] and Fromager *et al.* [30] without diffraction to study the temporal dynamics of lasers.

$$\frac{\partial E}{\partial \tau}=ia\Delta_{\perp}E+\sigma(P-E), \tag{2.1}$$

$$\frac{\partial P}{\partial \tau}=-[1+i(\delta+bD)]P+DE, \tag{2.2}$$

$$\frac{\partial D}{\partial \tau}=-\gamma\left[D-r+\frac{1}{2}(E^{*}P+EP^{*})\right]. \tag{2.3}$$

E, P, and D are the dimensionless envelopes of the electric field, the electric polarization and the population inversion, respectively. $\gamma\equiv\gamma_{\parallel}/\gamma_{\perp}$ and $\sigma=\kappa/\gamma_{\perp}$ are the population inversion decay rate and the cavity losses, respectively, in units of the polarization decay rate ($\gamma_{\perp}$). $\delta=(\omega_{21}-\omega)/\gamma_{\perp}$ is the rescaled detuning between the atomic line center and the fast oscillation of the laser field. r represents the pumping parameter. The spatial transverse size of the laser is L. Light diffraction is taken into account by means of the transverse Laplacian term in the field equation, and is measured by the diffraction coefficient $a=c^2/(2\omega\gamma_{\perp}d^2)$, where d is a characteristic spatial scale in the transverse plane. The value of d was chosen to be $L=9d$ for practical purposes in the numerical simulations. $\Delta_{\perp}=\partial_x^2+\partial_y^2$ is the transverse Laplacian where x and y are normalized with the spatial scale d. The time τ is normalized versus the polarization decay rate ($\tau=\gamma_{\perp}t$). The dimensionless parameter b measured the strength of the near dipole-dipole interactions. The usual value of this parameter, that is, without permanent dipole moments, is $2\kappa/(3\omega)$ [35,29,30]. It has been pointed out in previous works that a bad cavity condition is necessary in order to obtain an appreciable effect [29–31]. Unless we impose this condition of bad cavity, with a frequency not very large, the value of the NDD parameter will be too small to produce visible effects. However, if we consider active molecules with permanent dipole moments, the b parameter reads

$$b=\frac{2\kappa}{3\omega}-\frac{\kappa(\mu_{22}-\mu_{11})^2}{3\omega\mu_{12}^2}, \tag{2.4}$$

where μ_{12} is the transition dipole moment and μ_{22} and μ_{11} are the permanent dipole moments of the excited and ground level, respectively. Now, the presence of the permanent dipole moments allows us to obtain a significant effect of the local-field correction avoiding the restriction of the bad cavity condition. The active molecules suitable to show this behavior must have a large difference between their permanent dipole moments. As we have mentioned in the Introduction, they are in general, organic compounds with high polarizabilities, presenting significant nonlinear optical properties [17,37]. Some types of biomolecules also have high permanent dipole moments [38,39]. Another example is the ''dipole gas,'' that is, a gaseous medium of atoms or molecules possessing permanent dipole moments that may consist of hydrogen atoms [40]. Note that the NDD parameter b can take positive or negative values depending on the relevance of the permanent dipole moments. We will see in the following section that how this change of sign of b leads to a change of the behavior of the system.

III. STABILITY OF THE NONLASING SOLUTION

Let us analyze the stability of the nonlasing solution $E=0$, $P=0$, $D=r$. Following the same procedure as in Ref. [7], we linearize Eqs. (2.1)–(2.3) about this trivial solution and expand the variables as a Fourier series of transversal modes of wave vectors k. Then, we obtain the following instability condition from Eq. (A9), (see derivation in Appendix A):

$$\begin{aligned}G(r,k^2)\equiv{}&b^2r^2+[2b(\delta-ak^2)-(1+\sigma)^2]r+(1+\sigma)^2\\&+(\delta-ak^2)^2\\<{}&0.\end{aligned} \tag{3.1}$$

We clearly observe that the instability condition is a quadratic function of r. Therefore, it is verified for values of r in the range limited by the two real roots

$$r_{\pm}(k)=\frac{1}{2b^2}\left\{-2b(\delta-ak^2)+(1+\sigma)^2\pm(1+\sigma)^2\times\sqrt{1-\frac{4b}{(1+\sigma)^2}(\delta+b-ak^2)}\right\}, \tag{3.2}$$

therefore, the nonlasing solution will be unstable when the normalized pump verifies $r_-(k)<r<r_+(k)$. As we will see in the following section, there are two traveling-wave solutions, $E_{st\pm}$ [see Eq. (4.2)], due to the LFC, $r_{\pm}(k)$ being their corresponding thresholds. This result was previously shown in the case without laser field diffraction [29,30] and is related with the intrinsic bistability induced by the LFC. As it was pointed out in those works [29,30], at moderate values of the NDD parameter the threshold r_+ is much larger than r_-. In the following, we will focus our attention on the neutral stability curve $r_-(k)$. The minimum value of $r_-(k)$ occurs for the traveling wave with the lowest threshold (critical wave), that is, for the solution expected at the first laser threshold. Its corresponding wave vector is termed k_c. From the derivative $\partial r_-(k)/\partial k=0$ we obtain the solution $k=0$ and $k^2=(\delta+b)/a$. At this point, we consider the following two cases.

(a) $\delta<-b$: In this case, only the solution $k=0$ has physical meaning, hence a spatially uniform solution is expected at the laser threshold [see Figs. 1(a) and 2(a)]. The value of the threshold, termed r_c, is then

$$r_c\equiv r_-(k_c=0)=\frac{1}{2b^2}\left\{-2b\delta+(1+\sigma)^2-(1+\sigma)^2\times\sqrt{1-\frac{4b}{(1+\sigma)^2}(\delta+b)}\right\}. \tag{3.3}$$

(b) $\delta>-b$: In this case, it can be seen that the minimum value of $r_-(k)$ is for the other solution $k^2=(\delta+b)/a$, hence $k_c=\sqrt{(\delta+b)/a}$ and traveling waves with $\pm k_c$ are expected at the laser threshold [see Figs. 1(b), 1(c), and 2(b)]. The value of the threshold is $r_c\equiv r_-(k_c)=1$.

In summary, we have found that the laser emission is off-axis when the sum of the cavity detuning and the NDD parameter is larger than zero. It seems that the transverse solution selected at threshold is determined by the sign of the effective detuning $\delta_{\text{eff}}\equiv\delta+b$. Now, transverse traveling waves can occur even when the lasing frequency is larger than the transition frequency. This can be understood considering that the atomic line center shifts to a different value due to the LFC. As we mentioned above, the value of b can take positive or negative values depending on the strength of the permanent dipole moments, favoring the travelling wave if they have no significant contribution ($b>0$) or favoring the homogeneous solution if they are relevant ($b<0$).

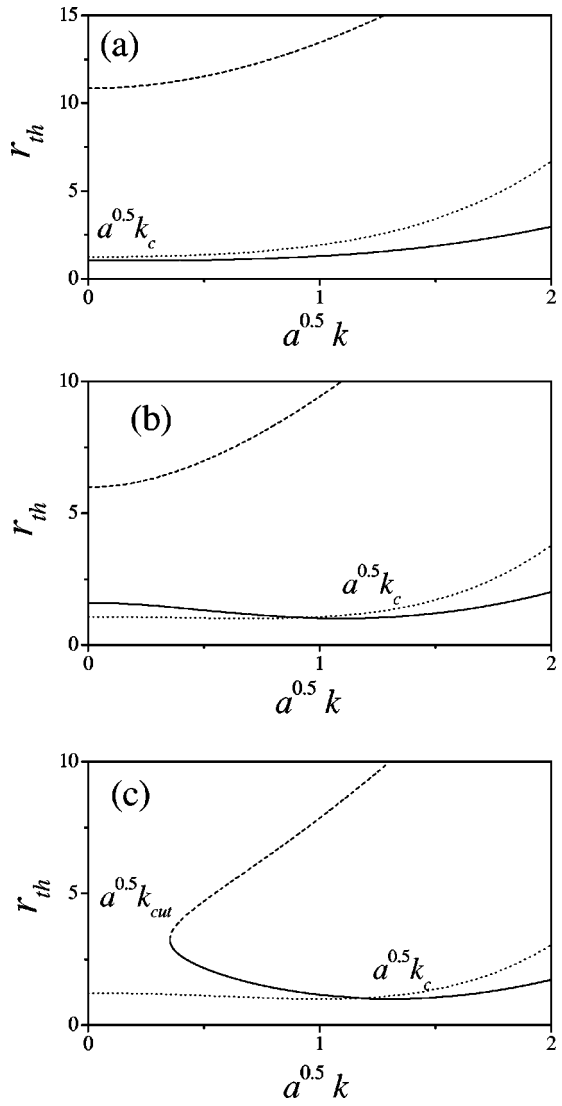

FIG. 1. General shape of the neutral stability curve, r_- (solid line) and r_+ (dashed line), vs the wave vector $a^{0.5}k$ for a detuning value (a) $\delta=-1<-b$, (b) $-b<\delta=0.5<\delta_0$, and (c) $\delta=1>\delta_0$. The parameter values are $\sigma=1.1$ and $b=0.7$. The case without LFC ($b=0$) is also shown (dotted line). All these magnitudes are dimensionless.

Another interesting feature that arises when the LFC is taken into account is the appearance of a cutoff in the laser field spectrum. The value of the cut-off is deduced from the necessary condition for $r_{\pm}$ [see Eq. (3.2)] to be real,

$$(1+\sigma)^2-4b(\delta+b-ak^2)\geqslant 0. \tag{3.4}$$

The condition (3.4) leads to a different result depending on the sign of the NDD parameter b. This condition implies a lower limit ($b>0$), or an upper limit ($b<0$), to the value of k, that is, to the size of the transverse structures that can appear in the laser dynamics. The expression of this cutoff can be easily found from Eq. (3.4),

$$k_{cut}^2\equiv\frac{1}{a}\left(\delta+b-\frac{(1+\sigma)^2}{4b}\right). \tag{3.5}$$

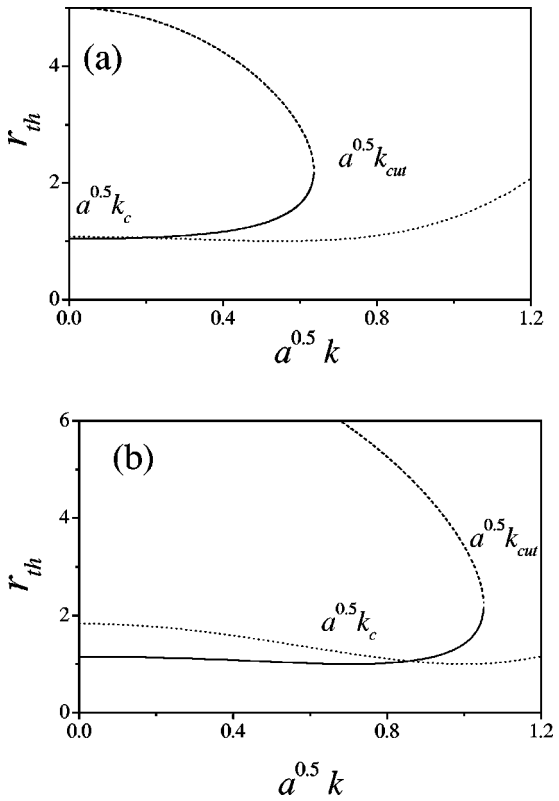

FIG. 2. General shape of the neutral stability curve, r_- (solid line) and r_+ (dashed line), vs the wave vector $a^{0.5}k$ for a detuning value (a) $\delta_0<\delta=0.3<-b$ and (b) $\delta=1>-b$. The parameter values are $\sigma=0.1$ and $b=-0.5$. The case without LFC ($b=0$) is also shown (dotted line). All these magnitudes are dimensionless.

We analyze the consequences of this result for positive and negative values of the NDD parameter. At $b>0$ the unstable condition (3.4) leads to a lower cutoff in the electric-field spectrum, that is, only the traveling waves whose wave vectors k^2 are larger than k_{cut}^2 are able to make unstable the nonlasing solution. This result provides the maximum spatial scale that can appear in the transverse pattern $2\pi/k_{cut}$. Only if $k_{cut}^2>0$, a cutoff in the field spectrum appears [see Fig. 1(c)]. This occurs when the cavity detuning is larger than a threshold value, i.e., $\delta>\delta_0$, where δ_0 reads

$$\delta_0 \equiv -b+\frac{(1+\sigma)^2}{4b}, \tag{3.6}$$

otherwise, all the spatial scales are able to make unstable the nonlasing solution [see Fig. 1(b)]. At $b<0$, that is, when the permanent dipole moments play an important role, instead of a lower limit in the electric-field spectrum, an upper limit arises. Then, only the waves whose wave vectors k^2 are lower than k_{cut}^2 are able to make unstable the nonlasing solution. In this case, it is essential that $k_{cut}^2>0$ in order to find a traveling wave that makes unstable the nonlasing solution. In other words, the detuning must be larger than δ_0 [see Eq. (3.6)] to obtain laser emission, otherwise laser emission cannot be obtained, however much the pump be increased. This phenomenon, due to the permanent dipole moments through the LFC, provides the minimum spatial scale, $2\pi/k_{cut}$ that can appear in the transverse pattern [see Fig. 2(b)].

We plot the general shape of the neutral stability curve, $r_-(k)$ and $r_+(k)$, in Fig. 1 for a positive value of b, and in Fig. 2 for a negative value of b. In all cases, we also plot the neutral stability curve without LFC for comparison purposes.

IV. SOLUTION ABOVE THRESHOLD: LINEAR STABILITY ANALYSIS OF THE LASING SOLUTION

The system admits, above threshold, traveling-wave solutions of the form

$$E=E_{st}e^{i(\vec{k}\cdot\vec{x}+\omega_{st}\tau)},\quad P=P_{st}e^{i(\vec{k}\cdot\vec{x}+\omega_{st}\tau)},\quad D=D_{st}, \tag{4.1}$$

where E_{st} and D_{st} are real numbers, whereas P_{st} is a complex quantity. Introducing the expressions (4.1) in Eqs. (2.1)–(2.3) we found two solutions for the variable E_{st}^2,

$$E_{st\pm}^2=r-r_\pm(k), \tag{4.2}$$

and the magnitudes ω_{st}, D_{st}, and P_{st} verifying

$$\omega_{st\pm}=-\frac{b\sigma r_\pm+\sigma\delta+ak^2}{1+\sigma},\quad D_{st\pm}=r_\pm,$$

$$P_{st\pm}=\left(1+i\frac{\omega_{st\pm}+ak^2}{\sigma}\right)E_{st\pm}. \tag{4.3}$$

Note that only the traveling waves with $k^2>k_{cut}^2$ (if $b>0$), or $k^2<k_{cut}^2$ (if $b<0$) are solutions of the system. The LFC leads to the existence of two traveling wave solutions. The solution E_{st-} that appears for $r>r_-$ and a second one (E_{st+}) that appears for $r>r_+$. As we mentioned above, this result was previously shown in the case without diffraction [29,30] and is related with the intrinsic bistability induced by the LFC. For the range of pump values used in this work, the nonlasing unstable band ($r_-<r<r_+$), only the the solution E_{st-} has a physical meaning. In the following, we eliminate the minus sign subindex from this traveling-wave solution.

We are going to study the stability of these transverse solutions to finite side-band perturbations by linearizing about the traveling-wave solution given by Eq. (4.1). This stability analysis was originally performed by Jakobsen *et al.* [7] and Lega *et al.* [14]:

$$E_s=(E_{st}+e_1e^{i\vec{q}\cdot\vec{x}}+e_2e^{-i\vec{q}\cdot\vec{x}})e^{i(\vec{k}\cdot\vec{x}+\omega_{st}\tau)},$$

$$P_s=(P_{st}+p_1e^{i\vec{q}\cdot\vec{x}}+p_2e^{-i\vec{q}\cdot\vec{x}})e^{i(\vec{k}\cdot\vec{x}+\omega_{st}\tau)}, \tag{4.4}$$

$$D_s=D_{st}+de^{i\vec{q}\cdot\vec{x}}+d^*e^{-i\vec{q}\cdot\vec{x}},$$

where e_1, e_2, p_1, p_2, and d are the perturbations, and $\vec{q}$ is the perturbation wave vector. Then we obtain $\partial_\tau\vec{v}=\mathcal{M}(\vec{k},\vec{q},r)\vec{v}$, where $\mathcal{M}$ is a 5×5 matrix and $\vec{v}$ denotes the column vector $(e_1,e_2^*,p_1,p_2^*,d)^T$. The time dependence of $\vec{v}$ is chosen as $e^{\lambda\tau}$, λ being the eigenvalues of $\mathcal{M}$. For a

given $\vec{k}$ and r, the traveling-wave solution is stable if, for all values of $\vec{q}$, the matrix of the coefficients $\mathcal{M}$ has all its eigenvalues with negative real part. If any eigenvalue has a positive real part, the solution represented by $(\vec{k},r)$ is unstable. The problem of finding the eigenvalues of the 5×5 matrix has been approached numerically. Let us now calculate the stability boundaries of the traveling waves in the $(\vec{k},r)$ plane. Note that we have to assume a direction for the traveling wave $\vec{k}$ and consider perturbations at arbitrary directions relative to the fixed direction. Here, we will consider two cases; perturbations occurring along the direction of the traveling wave ($\vec{q}$ parallel to $\vec{k}$) which give one-dimensional (1D) instabilities, and perturbations occurring at right angles of the traveling wave ($\vec{q}$ perpendicular to $\vec{k}$) which give 2D instabilities. In both cases, instabilities that correspond to modes that are neutral (eigenvalue with vanishing real part at $q=0$), are identified as phase instabilities [7]. This type of instability occurs at long wavelengths. On the other hand, instabilities that correspond to modes that are not neutral at $q=0$ are identified as amplitude instabilities [7]. Amplitude instabilities occur at short wavelengths. Of the phase instabilities, the Eckhaus instability, occurring along the direction of the traveling wave (1D instability), and the zigzag instability, occurring at right angles to the traveling wave direction (2D instability), are the most common. A variety of amplitude instabilities have been found in 1D both near and well beyond lasing threshold [5].

Let us now to consider the following parameters; $\sigma=1$, $\gamma=0.1$, and $a=0.01$. Feng *et al.* used similar parameters to study the stability of transverse traveling waves in the usual case without LFC [5]. In that work, the analysis was restricted to the case of one transverse dimension, and they found a new class of amplitude instabilities. First of all and for comparison purpose, we calculate the Busse balloon for the case without LFC, i.e., $b=0$. Figure 3 shows the parallel and perpendicular instability boundaries above the neutral stability curve for the case without LFC. We have chosen a positive detuning ($\delta=1$), where a traveling wave with wave vector $\sqrt{a}k_c=\sqrt{\delta}=1$ is selected above lasing threshold. In agreement with Ref. [7] we find a Eckhaus unstable band symmetrically placed around the critical traveling wave [see Fig. 3(a) (dotted line)]. However, the stable boundary of traveling waves due to 1D instabilities is defined by amplitude instabilities [see Fig. 3(a) (dashed line)]. A zigzag unstable band occurs to the immediate left of the critical traveling wave and extends all the way to the left boundary out to the neutral stability curve [see Fig. 3(b)]. This is the dominant instability occurring at right angles to the traveling-wave direction (2D instabilities).

The LFC induces several changes in the stability of the traveling waves. We first analyze the case where the difference between the permanent dipole moments is large, which gives a negative value of b. The Busse balloon at similar parameter values than above, but with negative NDD parameter ($b=-0.5$) is shown in Fig. 4. As we showed in the preceding section, a traveling wave is selected above the laser threshold with wave vector $\sqrt{a}k_c=\sqrt{\delta+b}\simeq0.7$. In

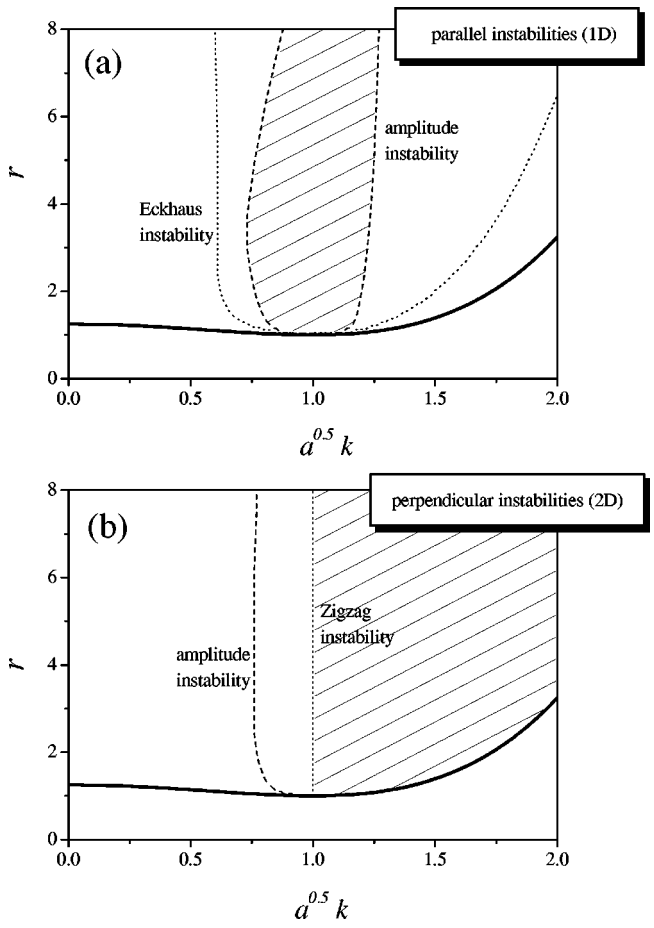

FIG. 3. Phase (dotted line) and amplitude (dashed line) instabilities corresponding to (a) parallel (1D) instabilities and (b) perpendicular (2D) instabilities in the $(\vec{k},r)$ plane. Both magnitudes are dimensionless. The traced area indicates the stable region of traveling waves including both the phase and amplitude instabilities. The neutral stability curve (solid line) is also shown. Case without LFC, i.e., $b=0$. The parameters are $\sigma=1$, $\gamma=0.1$, and $\delta=1$.

concern of the parallel perturbations, we observe a similar behavior than in the usual case without LFC; the stable boundary of traveling waves is defined by amplitude instabilities [see Fig. 4(a) (dashed line)]. However, this stable band is not symmetrically placed around the critical traveling wave. Now, traveling waves with wave vector lower than the critical one are 1D unstable. A more interesting result is found in the case of perpendicular perturbations [see Fig. 4(b)]. The LFC has removed the zigzag instability. Instead of this, an amplitude instability define the 2D stable region of traveling waves. We have found that the LFC at $b<0$ changes the nature of the instability boundary occurring at right angles to the traveling-wave direction. Let us analyze the case with positive b, that is, when the permanent dipole moments do not have a relevant contribution. A positive value of the NDD parameter can also modify the stability picture significantly. The Busse balloon at similar parameter values but with $b=0.5$ is shown in Fig. 5. The right boundary of the 1D stable region is defined by amplitude instabilities, as it happens in the usual case without LFC. However, the left boundary is a combination of Eckhaus (phase) and

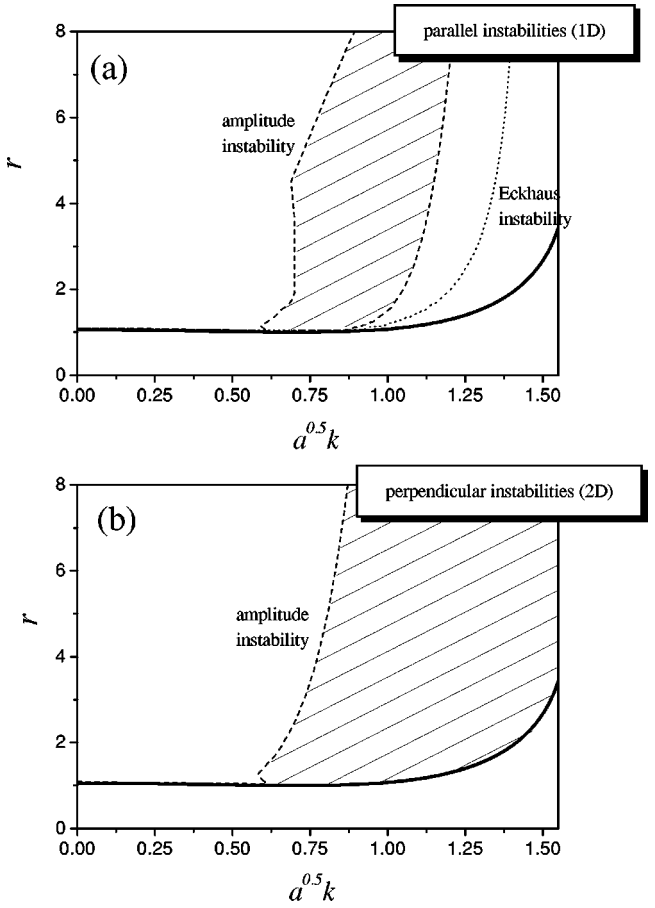

FIG. 4. Phase (dotted line) and amplitude (dashed line) instabilities corresponding to (a) parallel (1D) instabilities and (b) perpendicular (2D) instabilities in the $(\vec{k},r)$ plane. Both magnitudes are dimensionless. The traced area indicates the stable region of traveling waves including both the phase and amplitude instabilities. The neutral stability curve (solid line) is also shown. Case with negative NDD parameter, $b=-0.5$. The parameters are $\sigma=1$, $\gamma=0.1$, and $\delta=1$.

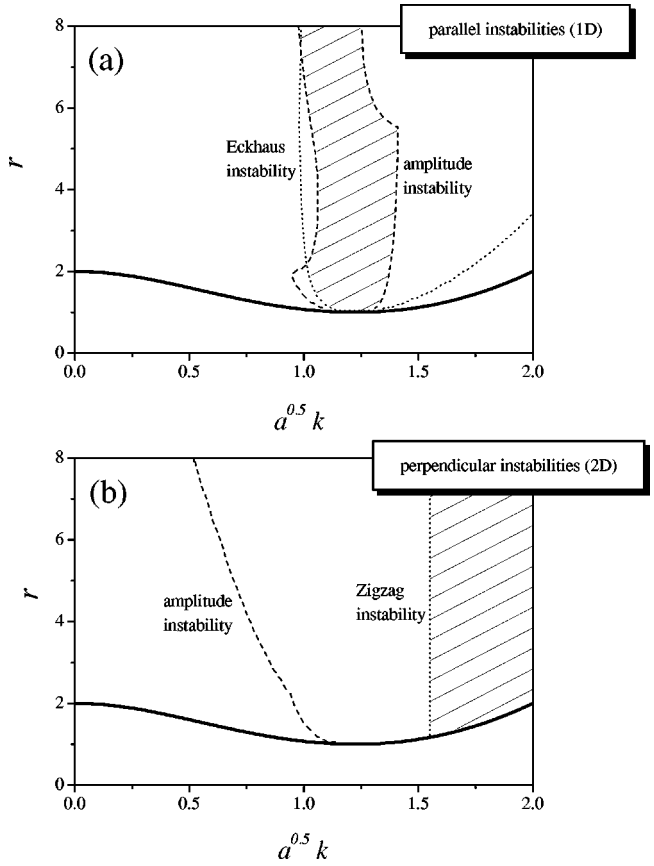

FIG. 5. Phase (dotted line) and amplitude (dashed line) instabilities corresponding to (a) parallel (1D) instabilities and (b) perpendicular (2D) instabilities in the $(\vec{k},r)$ plane. Both magnitudes are dimensionless. The traced area indicates the stable region of traveling waves including both the phase and amplitude instabilities. The neutral stability curve (solid line) is also shown. Case with positive NDD parameter, $b=0.5$. The parameters are $\sigma=1$, $\gamma=0.1$, and $\delta=1$.

amplitude instabilities [see Fig. 5(a)]. The stable band is symmetrically placed around the critical traveling wave. The perpendicular instabilities are shown in Fig. 5(b). We observe that the usual zigzag unstable band has shifted to the right from its usual position at the critical wave vector, in our case $\sqrt{a}k_c=\sqrt{\delta+b}\simeq 1.2$. We must point out that if we consider simultaneously both instabilities; parallel and perpendicular, we find that there is not any stable traveling wave in the $(\vec{k},r)$ plane. It means that the LFC has removed the Busse balloon.

These results seem to indicate that a more complex behavior is expected when the LFC is taken into account. In order to show the characteristic patterns above threshold, we have carried out numerical simulations.

V. NUMERICAL SIMULATIONS

We have numerically integrated the Eqs. (2.1)–(2.3) in a square bidimensional lattice of 151×151 cells with periodic boundary conditions by means of a finite-difference algorithm. We have chosen a dimensionless cell size $\Delta x=0.06$ which allows a good representation of the traveling wave, that is, enough cells per wavelength and also enough number of phase rolls in the lattice. The system starts with small-amplitude random initial conditions and runs for times much larger than the characteristic relaxation times (final dimensionless time of the order of $\tau=2\times 10^5$).

We have analyzed the pattern formation using the same parameter values as in Sec. IV. We first solve the case without LFC, i.e., $b=0$. We used a detuning value $\delta=1$ and a pump value close to threshold ($r=1.1$). After an initial transient, the system reaches a steady state where a traveling-wave solution takes place. The phase field and the power spectrum are shown in Fig. 6. Its wave vector corresponds to the critical wave vector ($k_c=\sqrt{\delta/a}=10$). We have found a similar behavior at higher pump values ($r=1.2$).

As we have seen in the stability analysis of the traveling-wave solutions, a more complex behavior in the case with LFC is expected. We first analyze the case with negative NDD parameter ($b=-0.5$) for the pump value $r=1.1$. The stability analysis of this case was shown in Fig. 4. We find

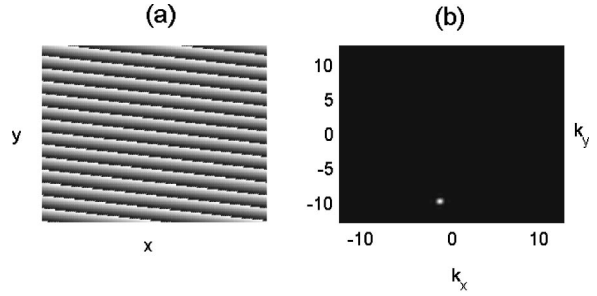

FIG. 6. (a) The phase field and (b) the power spectrum for the usual case without LFC, i.e., $b=0$. The parameters are $\sigma=1$, $\gamma=0.1$, $a=0.01$, $r=1.1$, and $\delta=1$. All the magnitudes presented in this figure are dimensionless [including the real (x,y) and the Fourier (k_x,k_y) space coordinates]. Note that the traveling-wave solution obtained in this case is characterized in the power spectrum by only one wave vector. This is due to the fact that the electric field that we are using in the Maxwell-Bloch equations (2.1)–(2.3) is the complex electric-field envelope, and therefore the traveling-wave solution [see Eq. (4.1)] is represented by only one wave vector (the complex conjugate component is not presented).

that the critical traveling-wave solution ($k_c=\sqrt{(\delta+b)/a}\simeq 7.1$) appears although a pair of optical vortices, i.e., dislocation defects in the phase structure [see Fig. 7(b) first row] accompanied by zeros in the intensity field [see Fig. 7(a) first row] are in the pattern. Figure 7 shows a sequence of three frames of the intensity field (a), the phase field (b), and the power spectrum (c). An interesting phenomenon can be observed in this sequence. In the first half of the time evolution, a traveling wave with some optical vortices takes place (Fig. 7, first row). The corresponding wave vector is the critical one (k_c), and the intensity field shows a constant profile with

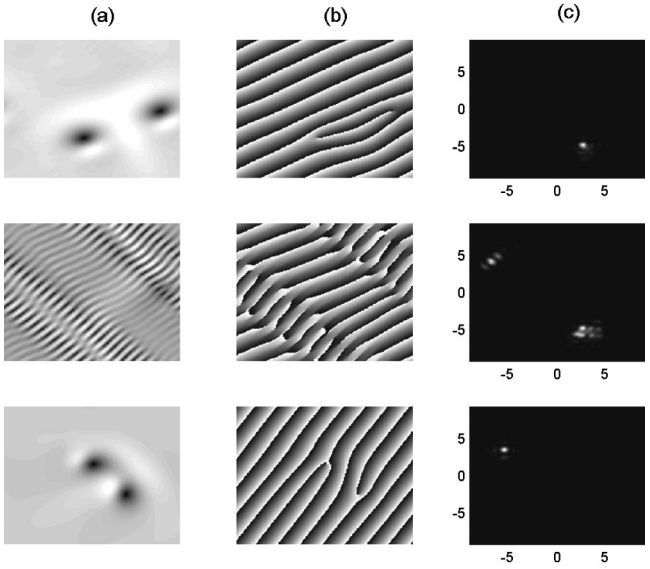

FIG. 7. Three frames from a movie showing (a) the intensity field, (b) the phase field, and (c) the power spectrum for the case with negative NDD parameter, $b=-0.5$. The parameters are $\sigma=1$, $\gamma=0.1$, $a=0.01$, $r=1.1$, and $\delta=1$. All the magnitudes presented in this figure are dimensionless [including the real (x,y) and the Fourier (k_x,k_y) space coordinates].

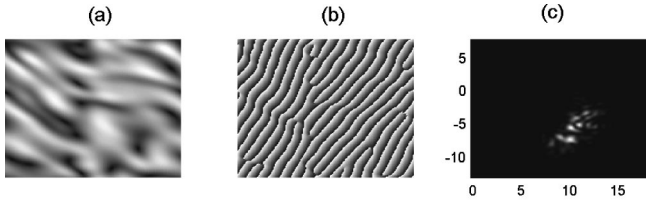

FIG. 8. (a) The intensity field, (b) the phase field, and (c) the power spectrum for the case with positive NDD parameter, $b=0.5$. The parameters are $\sigma=1$, $\gamma=0.1$, $a=0.01$, $r=1.1$, and $\delta=1$. All the magnitudes presented in this figure are dimensionless [including the real (x,y) and the Fourier (k_x,k_y) space coordinates].

two opposite topological charge optical vortices. After that, another tilted wave traveling near the opposite direction appears and the laser cross section breaks in different domains (Fig. 7, second row). Both waves have the same wave vector, k_c. These domains of tilted waves traveling at opposite directions are separated by a row of vortices [see Fig. 7(a) second row]. This is a transient regime of coexistence of two transversal structures in the pattern. Finally, the original wave disappears and the new one remains during the rest of the time evolution (Fig. 7, third row). In conclusion, we have seen a pattern formation mechanism in which the traveling-wave direction changes after a competition between the two waves. This phenomenon can mainly result from the parallel instability since this instability defines the global stable region of traveling wave in the $(\vec{k},r)$ plane. We have found that for an unstable traveling wave k, the parallel perturbation q that grows faster is such that the resulting wave vector is opposite to the critical one, i.e., $k-q\simeq -k_c$. By increasing the pump parameter to $r=1.2$, we find that this phenomenon (the change of traveling wave direction after competition of two opposite waves) is repeated in an irregular sequence.

To analyze the case with $b>0$, we have chosen the value $b=0.5$, with the same pump value $r=1.1$. The stability analysis was shown in Fig. 5. In this case, the power spectrum reveals that several traveling waves are in the transverse dynamics of the laser [see Fig. 8(c)]. Their corresponding wave vectors are placed around the critical wave vector ($k_c=\sqrt{(\delta+b)/a}\simeq 12$). The intensity field, the phase field, and the power spectrum are shown in Fig. 8. Several dislocation defects in the phase profile [see Fig. 8(b)], accompanied by zeros in the intensity field [see Fig. 8(a)] appear. These optical vortices remains during the whole evolution of the pattern, and also new spatial structures arise. These structures are larger than the critical transverse wave and appear in the intensity field [see Fig. 8(a)] as bright ridges aligned at right angles to the local traveling wave direction. As we have found in previous section, in this case ($b=0.5$) there is not any stable traveling wave. In particular, the critical traveling wave is unstable for perpendicular perturbations. Therefore, spatial structures perpendicular to the critical traveling wave are expected.

VI. CONCLUSIONS

The local-field correction in the laser transverse dynamics has been analyzed considering the presence of active mol-

ecules with permanent electric dipole moments. This local-field correction arises from near dipole-dipole interactions in a dense medium. This correction leads to a nonlinear term in the semiclassical Maxwell-Bloch equations which can be interpreted as a detuning depending on the population inversion. As it is well known, this term leads to the so-called intrinsic optical bistability .

The neutral stability curve obtained in the linear stability analysis of the nonlasing state depends now on the near dipole-dipole parameter b. This parameter can take positive or negative values depending on the relevance of the permanent dipole moments. The presence of the LFC shifts the value of the detuning that separates at threshold the traveling-wave solution from the homogeneous one to a negative value (if b is positive) or to a positive one (if b is negative). Therefore, the LFC favors the traveling wave if $b>0$ or the homogeneous solution if $b<0$. A lower cutoff when $b>0$ was found (an upper cutoff was found when $b<0$) in the laser field spectrum, which provides the maximum (minimum) spatial scale that can appear in the transverse pattern.

We have calculated the stability boundaries of the traveling waves, i.e., the Busse balloon. We found that the near dipole-dipole interactions modified the stability picture significantly. We have analyzed the stability when the NDD parameter takes a negative value and we found that the Busse balloon is delimited by amplitude instabilities occurring along the direction the traveling wave, as in the usual case without LFC, and at right angles to the traveling wave direction. Therefore, we have found a 2D instability in the laser dynamics. We have also studied the stability at positive values of the NDD parameter. The usual zigzag unstable band shifts to the right from its usual position at the critical wave vector. This means that the Busse balloon is removed by the LFC. Finally, we have carried out numerical simulations of the system. We observed close to the threshold that the LFC favors the growth of defects in the pattern. At negative NDD parameter, we found domains of tilted waves traveling at opposite directions separated by a row of vortices. As a result of this setup, a new transverse solution traveling at the opposite direction replaces the original one.

ACKNOWLEDGMENTS

We are very grateful to I. Gonzalo for his helpful advice and to T. Lorca for the correction of the manuscript. This work was supported by Project No. BFM2000-0796 (Spain).

APPENDIX: LINEAR STABILITY ANALYSIS OF THE NONLASING SOLUTION

In order to analyze the nonlasing solution ($E=P=0$, $D=r$), we linearize the laser equations (2.1)–(2.3) about the trivial solution and expand the variables as a Fourier series of transversal modes of wave vectors k. Therefore, we get for each set of Fourier components (E_k, P_k, D_k) the following system:

$$\frac{\partial E_k}{\partial \tau} = -iak^2 E_k + \sigma(P_k - E_k), \tag{A1}$$

$$\frac{\partial P_k}{\partial \tau} = -[1 + i(\delta + br)]P_k + rE_k, \tag{A2}$$

$$\frac{\partial D_k}{\partial \tau} = -\gamma D_k, \tag{A3}$$

which yields the three eigenvalues,

$$\lambda_3 = -\gamma, \tag{A4}$$

$$\lambda_{\pm} = -\frac{1+\sigma+i(\delta+br+ak^2)}{2} \pm \sqrt{\left(\frac{1-\sigma+i(\delta+br-ak^2)}{2}\right)^2 + \sigma r}. \tag{A5}$$

The trivial solution is linearly unstable if one of the eigenvalues has a positive real part. The expression under the square root is a complex number that will be denoted by $(\chi+i\xi)^2$, with $\chi \geqslant 0$, namely,

$$(\chi+i\xi)^2 \equiv \left(\frac{1-\sigma+i(\delta+br-ak^2)}{2}\right)^2 + \sigma r. \tag{A6}$$

It can be seen that the trivial solution is unstable if and only if the real part of Eq. (A5) is positive, i.e., $-((1+\sigma)/2) \pm \chi > 0$, equivalent to $\chi^2 > ((1+\sigma)/2)^2$. Equating the real and imaginary parts on both sides of Eq. (A6) we find that χ satisfies

$$F(\chi^2) \equiv \chi^4 - \left[\left(\frac{1-\sigma}{2}\right)^2 - \left(\frac{\delta+br-ak^2}{2}\right)^2 + \sigma r\right]\chi^2 - \left(\frac{1-\sigma}{2}\right)^2\left(\frac{\delta+br-ak^2}{2}\right)^2 = 0. \tag{A7}$$

This expression can be interpreted as a function of a variable, $F(\theta^2)$, which has a real and positive zero for $\theta^2=\chi^2$. It can be seen that the parabola $F(\theta^2)$ has two real zeros, one of them positive and the other negative, but only the positive one has a physical meaning since χ is defined as real and then χ^2 must be positive. Hence, $F(\theta^2)<0$ for $\theta^2<\chi^2$. In particular, if $[(1+\sigma)/2]^2<\chi^2$ (the above instability condition), the function F takes a negative value for $\theta^2=[(1+\sigma)/2]^2$. Thus, when χ^2 is replaced by $[(1+\sigma)/2]^2$ in Eq. (A7), we have the instability condition,

$$F([(1+\sigma)/2]^2) \equiv \frac{\sigma}{4}[(1+\sigma)^2 + (\delta+br-ak^2)^2 - r(1+\sigma)^2] < 0, \tag{A8}$$

which can be rearranged to read

$$G(r,k^2) \equiv (1+\sigma)^2(1-r) + (\delta+br-ak^2)^2 < 0. \tag{A9}$$

It is easy to see that the normalized pump r must verify $r>1$ for Eq. (A9) to be fulfilled.

[1] P.K. Jakobsen, J.V. Moloney, A.C. Newell, and R. Indik, Phys. Rev. A **45**, 8129 (1992).
[2] A.C. Newell and J.V. Moloney, *Nonlinear Optics* (Addison-Wesley, Redwood City, CA, 1992).
[3] E.J. D'Angelo, E. Izaguirre, G.B. Mindlin, G. Huyet, L. Gil, and J.R. Tredicce, Phys. Rev. Lett. **68**, 3702 (1992).
[4] F.T. Arecchi, S. Boccaletti, P.L. Ramazza, and S. Residori, Phys. Rev. Lett. **70**, 2277 (1993).
[5] Q. Feng, J.V. Moloney, and A.C. Newell, Phys. Rev. Lett. **71**, 1705 (1993).
[6] F. Prati, M. Brambilla, and L.A. Lugiato, Riv. Nuovo Cimento **17**, 1 (1994).
[7] P.K. Jakobsen, J. Lega, Q. Feng, M. Staley, J.V. Moloney, and A.C. Newell, Phys. Rev. A **49**, 4189 (1994).
[8] G. Huyet, M.C. Martinoni, J.R. Tredicce, and S. Rica, Phys. Rev. Lett. **75**, 4027 (1995).
[9] V.M. Pérez-García, I. Pastor, and J.M. Guerra, Phys. Rev. A **52**, 2392 (1995).
[10] R. Herrero, E.G. Westhoff, A. Aumann, T. Ackemann, Y.A. Logvin, and W. Lange, Phys. Rev. Lett. **82**, 4627 (1999).
[11] R.S. Bennink, V. Wong, A.M. Marino, D.L. Aronstein, R.W. Boyd, C.R. Stroud, Jr., S. Lakishova, and D.J. Gauthier, Phys. Rev. Lett. **88**, 113901 (2002).
[12] Chaos, Solitons Fractals **10**(4-5) 1999, special issue of the WE-Heraeus seminar on pattern formation in nonlinear optical systems.
[13] P. Coullet, L. Gil, and F. Rocca, Opt. Commun. **73**, 403 (1989).
[14] J. Lega, P.K. Jakobsen, J.V. Moloney, and A.C. Newell, Phys. Rev. A **49**, 4201 (1994).
[15] K. Staliunas, G. Slekys, and C.O. Weiss, Phys. Rev. Lett. **79**, 2658 (1997).
[16] S.P. Hegarty, G. Huyet, and J.G. McInerney, Phys. Rev. Lett. **82**, 1434 (1999).
[17] N.C. Kothari and T. Kobayashi, IEEE J. Quantum Electron. **20**, 418 (1984).
[18] C.M. Bowden, A. Postan, and R. Inguva, J. Opt. Soc. Am. B **8**, 1081 (1991).
[19] C.R. Stroud, C.M. Bowden, and L. Allen, Opt. Commun. **67**, 386 (1988).
[20] R. Friedberg, S.R. Hartmann, and J.T. Manasseh, Phys. Rep. **7**, 101 (1973); **39**, 3444 (1989); **40**, 2446 (1989).
[21] J.J. Maki, M.S. Malcuit, J.E. Sipe, and R.W. Boyd, Phys. Rev. Lett. **67**, 972 (1991).
[22] M.E. Crenshaw, M. Scalora, and C.M. Bowden, Phys. Rev. Lett. **68**, 911 (1992).
[23] F.A. Hopf, C.M. Bowden, and W. Louisell, Phys. Rev. A **29**, 2591 (1984).
[24] Y. Ben-Aryeh, C.M. Bowden, and J.C. Englund, Phys. Rev. A **34**, 3917 (1986).
[25] J.W. Haus, L. Wang, M. Scalora, and C.M. Bowden, Phys. Rev. A **38**, 4043 (1988).
[26] R. Inguva and C.M. Bowden, Phys. Rev. A **41**, 1670 (1990).
[27] M.P. Hehlen, H.U. Güdel, Q. Shu, J. Rai, S. Rai, and S.C. Rand, Phys. Rev. Lett. **73**, 1103 (1994).
[28] C.M. Bowden, Phys. World **7**, 24 (1994).
[29] F. Sanchez, M. Brunel, G. Martel, and K. Aït Ameur, Phys. Rev. A **61**, 033817 (2000).
[30] M. Fromager, M. Brunel, and F. Sanchez, Phys. Rev. A **61**, 053804 (2000).
[31] C.M. Bowden, S. Sing, and G.P. Agrawal, J. Mod. Opt. **42**, 101 (1995).
[32] V. Ahufinger, J. Mompart, R. Corbalan, J. Garcia-Ojalvo, M. C. Torrent, and R. Vilaseca, in Proceedings of the International Quantum Electronics Conference/Lasers, Applications and Technologies (IQEC/LAT 2002), Moscow, 2002 (unpublished).
[33] V. Ahufinger, J. Garcia-Ojalvo, J. Mompart, M.C. Torrent, R. Corbalan, and R. Vilaseca (unpublished).
[34] The presence of the permanent dipole moments has been considered in several works leading to appealing phenomena such as sharp features appearance in on-resonant one-photon or two-photon nonlinear absorption and dispersion, Refs. [17,37], M.A. Kmetic and W.J. Meath, Phys. Rev. A **41**, 1556 (1990), R. Bavli and Y.B. Band, *ibid.* **43**, 5039 (1991); direct two-photon transitions in a two-level system, Ref. [17], M.A. Antón and I. Gonzalo, IEEE J. Quantum Electron. **31**, 1088 (1995); microwave amplification through laser radiation [40]; high harmonic generation, Ref. [38], O.G. Calderón, R. Gutiérrez-Castrejón, and J.M. Guerra, IEEE J. Quantum Electron. **35**, 47 (1999); and optical bistability in lasers, O.G. Calderón, S. Melle, and I. Gonzalo, Phys. Rev. A **65**, 023811 (2002).
[35] A.A. Afanas'ev, R.A. Vlasov, N.B. Gubar, and V.M. Volkov, J. Opt. Soc. Am. B **15**, 1160 (1998).
[36] C.M. Bowden and P. Dowling, Phys. Rev. A **47**, 1247 (1993).
[37] T. Hattori and T. Kobayashi, Phys. Rev. A **35**, 2733 (1987).
[38] V.A. Kovarsky, B.S. Philipp, and E.V. Kovarsky, Phys. Lett. A **226**, 321 (1997).
[39] R.B. Setlow and E.C. Pollard, *Molecular Biophysics* (Addison-Wesley, London, 1962).
[40] V.P. Gavrilenko and E. Oks, Phys. Rev. Lett. **74**, 3796 (1995).